

Article

Re-Distribution of Welding Residual Stress in Fatigue Crack Propagation Considering Elastic–Plastic Behavior

Yuxuan Xia ¹ , Jingxia Yue ¹, Jiankang Lei ² , Ke Yang ³ and Yordan Garbatov ^{4,*} 

- ¹ School of Naval Architecture, Ocean and Energy Power Engineering, Wuhan University of Technology, Wuhan 430063, China; xmqzww1999@whut.edu.cn (Y.X.); j.yue@whut.edu.cn (J.Y.)
² Luoyang Ship Material Research Institute, Luoyang 471000, China; lejiankang@whut.edu.cn
³ Dongfang Electric Wind Power Co., Ltd., Deyang 618000, China; yangk0732@dongfang.com
⁴ Centre for Marine Technology and Ocean Engineering (CENTEC), Instituto Superior Técnico, Universidade de Lisboa, 1649-004 Lisboa, Portugal
* Correspondence: yordan.garbatov@tecnico.ulisboa.pt

Abstract: The welding residual stress re-distribution behavior during fatigue crack propagation in butt-welded high-strength steel plates for ship construction is investigated based on experimental test results and numerical analyses. The specimens' initial welding residual stresses are obtained from X-ray for middle tensile (MT) specimens cut from butt-welded high-strength steel plates. Then, fatigue crack propagation experiments on MT specimens are conducted, and a strain gauge is used to measure the residual stress re-distribution field around cracks. A practical fatigue crack propagation simulation procedure is developed with a dynamic update of in-situ welding residual stress, where the residual stress intensity factor K_{res} of the MT specimen is deduced. The stress ratio effect on K_{res} during fatigue crack propagation is analyzed and a good agreement between experimental and numerical results is achieved.

Keywords: fatigue crack propagation; welding residual stress; plastic re-distribution; stress ratio effect



Citation: Xia, Y.; Yue, J.; Lei, J.; Yang, K.; Garbatov, Y. Re-Distribution of Welding Residual Stress in Fatigue Crack Propagation Considering Elastic–Plastic Behavior. *J. Mar. Sci. Eng.* **2023**, *11*, 2378. <https://doi.org/10.3390/jmse11122378>

Academic Editor: Weicheng Cui

Received: 8 November 2023

Revised: 9 December 2023

Accepted: 14 December 2023

Published: 17 December 2023



Copyright: © 2023 by the authors. Licensee MDPI, Basel, Switzerland. This article is an open access article distributed under the terms and conditions of the Creative Commons Attribution (CC BY) license (<https://creativecommons.org/licenses/by/4.0/>).

1. Introduction

Welding is the main way of joining metal structures, but can result in fatigue failure due to the residual stresses generated. Additionally, due to the complexity of welding, initial defects like inclusion, porosity, undercut, lack of penetration, etc., are present, which may initiate cracks and growth under cyclic loadings [1]. The fracture mechanics approach may be used to study the fatigue life of cracked structures, which is considered suitable for assessing fatigue strength. The residual stress intensity factor K_{res} is used to quantify the effect of welding-induced residual stress (WRS) on crack propagation behavior. It is considered in calculating the effective stress intensity factor range ΔK_{eff} . Currently, there are two mainstream methods for the calculation of K_{res} : the weight function method (WFM) and the finite element method (FEM). The WFM can calculate K_{res} quickly based on the assumption of linear elasticity. At the same time, FEM can consider the effect of the material's plasticity, due to which it can obtain more accurate results.

Most studies have ignored the influence of WRS re-distribution, leading to the deviation between prediction and actual crack propagation behavior in the areas containing WRS [2]. WRS re-distribution behavior results from reducing the structure's remaining ligament during crack growth. Servetti and Zhang [3] calculated MT specimens' stress intensity factor (SIF) using a virtual crack technique with the static simulation of crack propagation in 0.5 mm increments of crack length. Barsoum and Barsoum [4] calculated the ΔK_{eff} of a T-shaped welded joint under the influence of WRS re-distribution using a 2D finite element method. Lee et al. [5] analyzed the variation in WRS during crack propagation, and found that the results were more accurate when considering the re-distribution behavior. Terada [6] proposed the WRS re-distribution rule for butt welding based on the superposition

principle and ideal residual stress distribution rule, which were in good agreement with experimental results. Xu [7] studied the crack propagation behavior of the butt-welded plate and found that the WRS was constantly released during crack propagation, with a decreasing impact on the crack propagation behavior.

The above studies used WRS re-distribution behavior during crack propagation by employing the linear elastic fracture mechanics (LEFM) method and proposed simplified approaches. However, the crack tip material yields due to the high stress concentration during the crack propagation process, and plastic strain will lead to further changes in areas containing WRS. Several studies have shown that the effect of plastic strain on WRS re-distribution at the crack tip is essential. The studies presented in [8–10] monitored the WRS re-distribution behaviors of MT and compact tension (CT) specimens through a neutron diffraction technique. They pointed out that neglecting the effect of plasticity would obtain inaccurate results. Wang and Qian [11] measured the residual stress of welded specimens, indicating that WRS relaxation depends on stress re-distribution caused by plastic deformation, and the plastic re-distribution behavior is affected by loading ratios. In experimental studies, XRD is often used as a means of measurement [12,13]. However, according to the existing studies, there is not a well-established method for assessing of WRS plastic re-distribution.

This research investigates the plastic re-distribution behavior of areas containing WRS and its effect on crack propagation behavior. This study uses experimental and simulation studies of WRS re-distribution behavior during fatigue crack propagation. The whole investigation is organized as follows: Section 2 introduces the crack propagation experiment of MT specimens and the theoretical calculation method of residual stress re-distribution. Deviations between experimental data and theoretical predictions are discussed. In Section 3, an elastic–plastic crack propagation simulation procedure of residual stress’s plastic re-distribution behavior is developed, and the comparison between experimental and numerical results is conducted to verify the accuracy and effectiveness of the proposed simulation method. Section 4 discusses the relation between K_{res} , and stress ratio R based on elastic–plastic simulation results. Finally, this study presented a polynomial prediction model to describe K_{res} by loading ratio R and crack size a/W . All conclusions are drawn in Section 5.

2. Experimental Procedure

A series of crack propagation experiments were conducted to establish an actual reference of crack propagation and the re-distribution behavior of WRS. Details of the experiments are described in the following content.

2.1. Material and Main Dimensions of Specimens

The material of specimens used in the experiments is Ni-Cr-Mo-V high-strength marine steel used for large ships and offshore structures. Table 1 lists the parameters of the Chaboche combined hardening model obtained through material experiments at room temperature.

Table 1. Material properties and Chaboche combined hardening model parameters of Ni-Cr-Mo-V.

E/GPa	ν	σ_{ys}/MPa	σ_u/MPa	σ_0/MPa	C_1	γ_1	C_2	γ_2
219	0.35	635	688	565	66,500	1485	950	14.25

MT-shape specimens were used to represent a classical butt-welded form, as shown in Figure 1. All specimens were manufactured as $300 \times 300 \times 12$ mm butt-welded square plates from the same Ni-Cr-Mo-V steel plate. The welding process used a flat butt submerged-arc technique with a Y-shaped bevel, and welding speed was controlled at 30–40 cm/min. The final average welded width is around 14 mm. As shown in Figure 1, the MT specimen was fabricated using laser cutting.

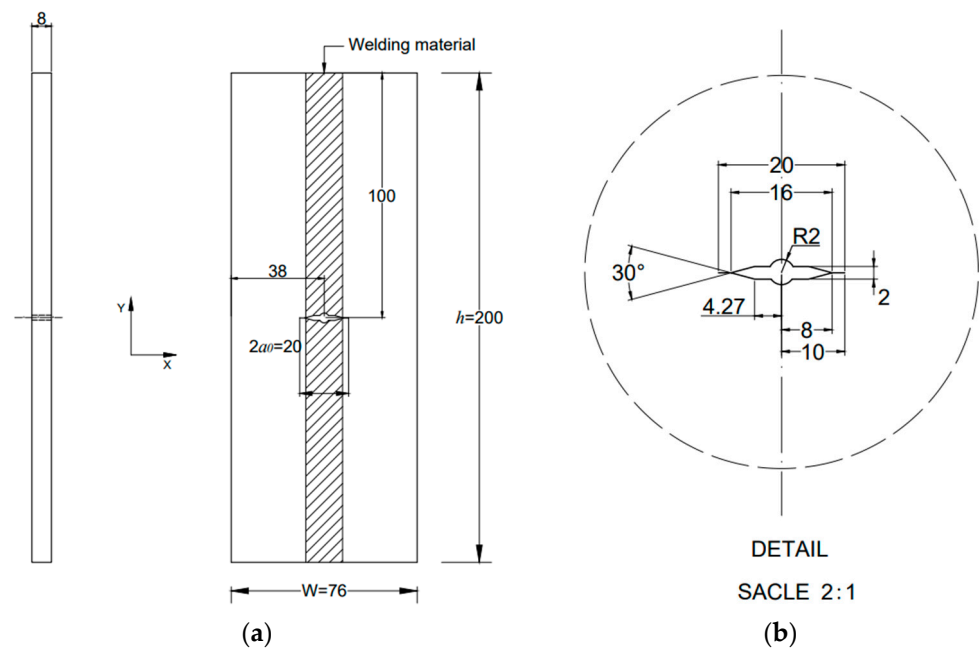


Figure 1. Geometry of the MT specimen: (a) global; (b) local detail. (Unit: mm).

Meanwhile, a 2 mm pre-crack was cut using a 0.12 mm molybdenum wire according to ASTM E647 [14]. It should be noted that this study only focused on the residual fatigue strength and crack propagation behavior in the base material of MT specimens. Those behaviors in the welded area were not investigated.

2.2. Test Setup

At the beginning of the fatigue experiment, the initial WRS of MT specimens was measured non-destructively using a portable X-ray stress detector, as shown in Figure 2. Due to the X-ray method's constraint, the initial stress states of MT specimens' surfaces are measured. Only longitudinal (y -direction) WRS distributions are concerned in the measurement, contributing to crack opening. Moreover, the measured path is set along the crack propagation direction (x -direction). Each point located far away from the welded zone has a 5 mm spacing, and spacing between other points near the weld is appropriately closer.

To investigate the influence of initial defect and butt welding on initial WRS, the following three types of MT specimens were designed and manufactured: (a) butt specimen without pre-cracks, (b) butt specimen with pre-cracks and (c) non-welded base material specimen with pre-cracks. For the butt specimen without pre-cracks, initial residual stresses were measured at three paths: center line C ($y = 0$), upper line U ($y = 15$), and back-center line C-Back ($y_B = 0$). For butt specimens with pre-cracks, only longitudinal residual stress distribution on the crack extension line was measured. The measurement paths and local coordinate systems on the specimen are illustrated in Figure 2. Residual stress data will be presented in Section 2.3.1.

A series of fatigue crack propagation experiments on MT specimens were conducted to investigate crack propagation behavior, and an initial residual stress was field obtained. All MT specimens were tested at room temperature in the JXG-200 high-frequency fatigue test machine with a maximum loading capacity of ± 300 kN. The applied load form is a sine wave applied along the weld direction. All loading conditions are listed in Table 2. The test machine's counterweight and the specimen's stiffness determined the loading frequency. During the experiment, the loading frequency was about 160 Hz when loading began and gradually decreased with the crack propagation.

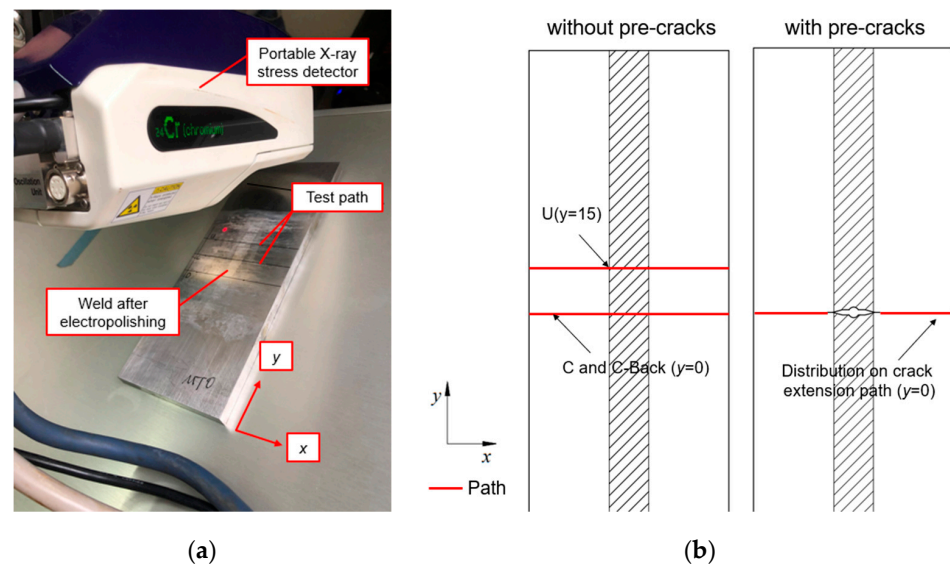


Figure 2. Measurement of initial residual stress (a) measurement device; (b) measurement paths.

Table 2. The loading condition of MT specimens.

Specimen Number	$\Delta\sigma_{nominal}/\text{MPa}$	R	Control Group Number
R – 0.1	100	–0.1	–
R0.1	100	0.1	R0.1-B
R0.3	100	0.3	R0.3-B
R0.5	100	0.5	R0.5-B

MT specimens were assembled, as shown in Figure 3. The actuator and clamp were aligned with the longitudinal central line of specimens before loading. During the experiment, strain gauges were used to monitor the change in residual strain along crack propagation, with the cracks being located at $x = -25, -15, 12$ and 22 mm, respectively. The loading was decreased to zero when data were collected. It should be noted that these operations may have a potential variable amplitude effect on crack propagation behavior and plastic zone at the crack tip, which is not discussed in the current study. A CCD camera measured the crack length, and loading cycles were recorded using a computer.

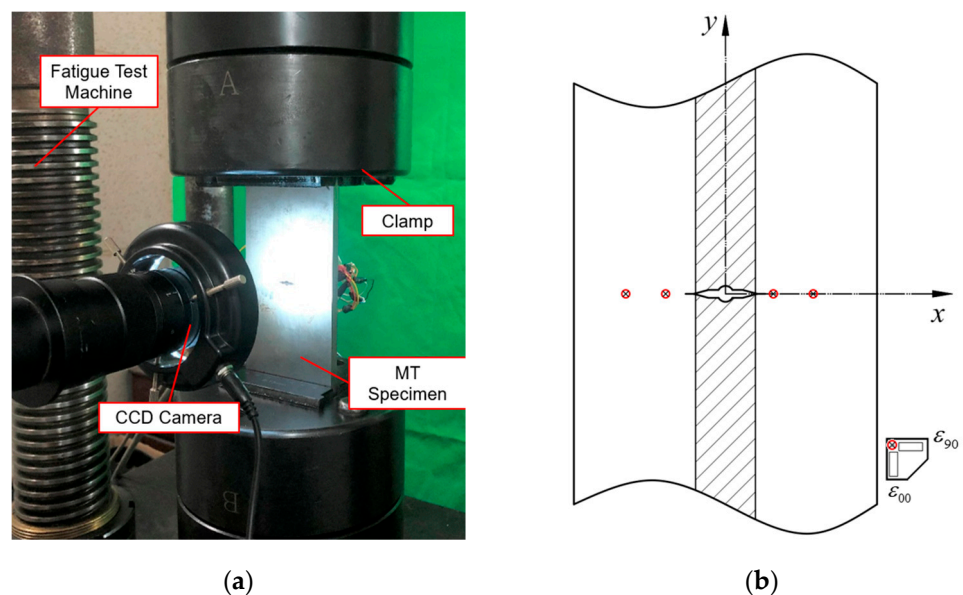


Figure 3. (a) Scheme of crack propagation experiment system; (b) measuring point layout.

2.3. Experimental Results and Discussion

2.3.1. Distribution of Initial Welding Residual Stress

The measurement results of longitudinal initial WRS σ_y for all specimens are given in this section. Firstly, the difference in the longitudinal initial WRS distribution of measurement paths of butt specimens without pre-cracks is discussed, as shown in Figure 4. The positions where the tension–compression stress converts or reaches peak value are close, and the deviation of initial WRS results of each measurement path was kept within 20 MPa. This phenomenon indicates that the stress distribution of WRS on the upper and lower surfaces is similar.

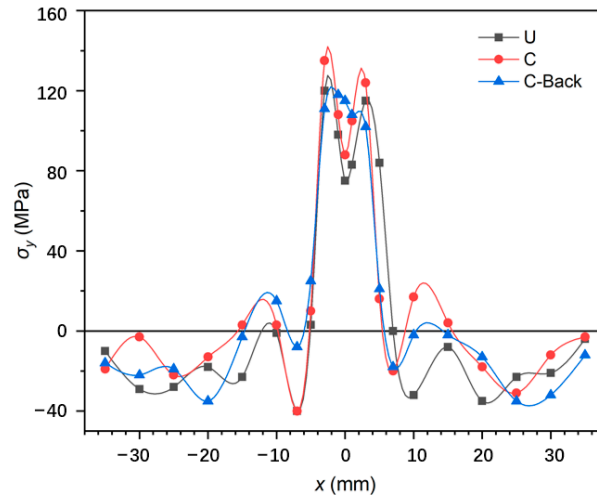


Figure 4. Initial WRS distribution at different paths of butt specimen without pre-cracks.

Then, two distribution function models were adopted: the Terada distribution function [15], as shown in Equation (1), and the Tada and Paris distribution function [16], as shown in Equation (2), to compare with the measured results (Path-C), as shown in Figure 5.

$$\sigma_y(x) = \sigma_{y,0} \exp^{-\frac{1}{2}(x/c)^2} [1 - (x/c)^2] \tag{1}$$

$$\sigma_y(x) = \sigma_{y,0} [1 - (x/c)^2] / [1 + (x/c)^4] \tag{2}$$

where x is the x coordinate value shown in Figure 3; $\sigma_{y,0} = 131$ MPa and $c = 8.94$ are the initial WRS distribution parameters obtained from X-ray measurement results.

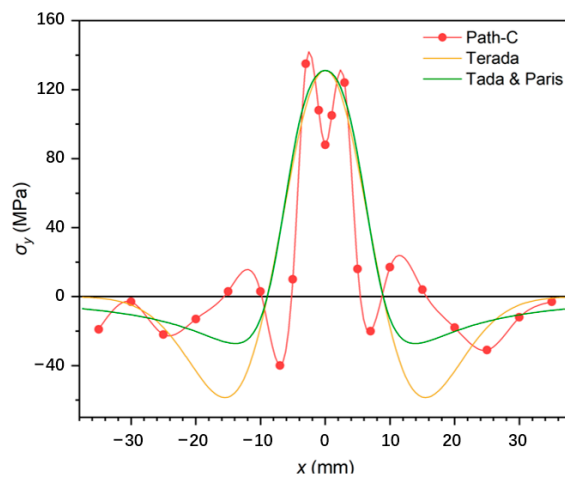


Figure 5. Initial WRS of butt specimen without pre-cracks found using X-ray and distribution function.

As illustrated in Figure 5, the measured data show an apparent bimodal feature. Stress in the center of the weld is lower than on two sides due to the annealing operation after the last welding. In contrast, distribution functions predict a unimodal distribution, unlike test data. At the edge of the specimen far away from the weld (where $x \geq 25$ mm), σ_y decreases to 0, and there is no significant difference between distribution functions and test data. The peaks of the two are also very close to each other, which indicates the reliability of the measurements.

The initial WRS of three types of specimens was compared in Figure 6. Compared with the butt specimen without pre-cracks (Path-C), the longitudinal WRS near the crack tip ($x = \pm 10$ mm) of the butt specimen with pre-cracks (MT-A) increases dramatically from 20 MPa to 60–120 MPa with the appearance of a crack. This is because when materials at the center of the specimen are removed, WRS needs to be balanced on the residual ligament of the specimen. Additionally, in the area far from the crack tip ($x = \pm 25$ mm), the residual compressive peak stress also increases to balance residual tensile stress near the crack tip. This phenomenon indicates that the WRS re-distribution caused by the crack length change cannot be ignored. As for the initial WRS of non-welded base material specimens with pre-cracks (MT-B), measured data are much closer to zero than MT-A.

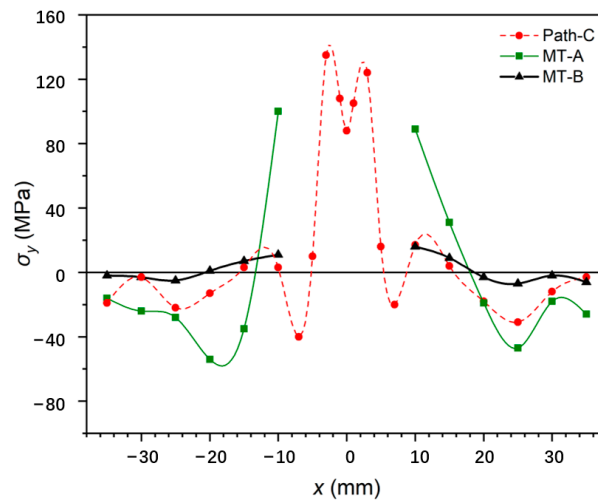


Figure 6. Initial WRS distribution of three types of MT specimen.

2.3.2. Welding Residual Stress Re-Distribution Calculation

Terada proposed the following rule as a theoretical solution to predict the WRS re-distribution behavior of butt-welded specimens:

$$\sigma_{y,re}(x) = \sigma_y(x) + \frac{a}{\pi\sqrt{x^2 - a^2}} \int_{-a}^a \sigma_y(\xi) \left(\frac{\sqrt{a^2 - \xi^2}}{x - \xi} + \frac{\sqrt{a^2 - \xi^2}}{x + \xi} \right) d\xi \quad (3)$$

where $\sigma_y(x)$ is the initial longitudinal WRS value calculated by Equation (2), $\sigma_{y,re}(x)$ is the longitudinal WRS re-distribution value, and a is the current crack length. It should be noted that both Equations (1) and (3) are named as Terada rules, Equation (1) is used to describe the distribution of the initial WRS and Equation (3) is used to describe the re-distribution of the WRS. To simplify the calculation, Terada [6] proposed a numerical integration approximation method:

$$\int_{-a}^a \sigma_y(\xi) \frac{\sqrt{a^2 - \xi^2}}{x \mp \xi} d\xi = a^2 \sum_{i=1}^n w_i \frac{\sigma_y(at_i)}{x \mp at_i} \quad (4)$$

and

$$t_i = \cos \frac{i\pi}{n + 1} \quad (5)$$

$$w_i = \frac{\pi}{n+1} \sin^2\left(\frac{i\pi}{n+1}\right) \tag{6}$$

where $n = 30$ is the numerical discretization parameter.

Terada rule can predict the re-distribution behavior of WRS when the initial distribution is determined. However, due to the singularity of integral multiplier $a/\pi(x^2 - a^2)^{1/2}$ at the crack tip, the accuracy of the Terada rule is not satisfying near the crack tip.

On the other hand, the experimental method is also an essential means of researching the re-distribution behavior of fatigue crack propagation. The experimental method is supported by measurements using bidirectional strain gauges, and generalized Hooke's law can derive the variation in residual stress $\Delta\sigma_y$ on the crack extension line:

$$\Delta\sigma_y = \frac{E}{1-\nu^2} [(\epsilon'_{00} - \epsilon_{00}) + (\epsilon'_{90} - \epsilon_{90})] \tag{7}$$

where $(\epsilon_{00} \ \epsilon_{90})$ and $(\epsilon'_{00} \ \epsilon'_{90})$ are the bidirectional strain gauge readings of measuring points on the crack extension line before and after crack propagation. The subscript "00" represents the direction parallel to the weld, and "90" represents the direction perpendicular to the weld. E and ν are Young's modulus and Poisson's ratio of the material, respectively.

The results of the experiment method and the Terada rule are compared in Figure 7. Predictions of the Terada rule keep the same growth rate and trend with the experiment method at the early and middle stages of crack propagation ($a = 10\sim 18$ mm). However, at the later stage of crack propagation ($a = 18\sim 25$ mm), when the crack tip becomes much closer to measuring points, the predicted result of the Terada rule changes to compressive stress while the experiment result is still in tension. The main reason for this phenomenon is that the Terada rule neglects the plastic deformation effect on residual stress near the crack tip and regards that the detachment of the crack surface quickly releases residual stress.

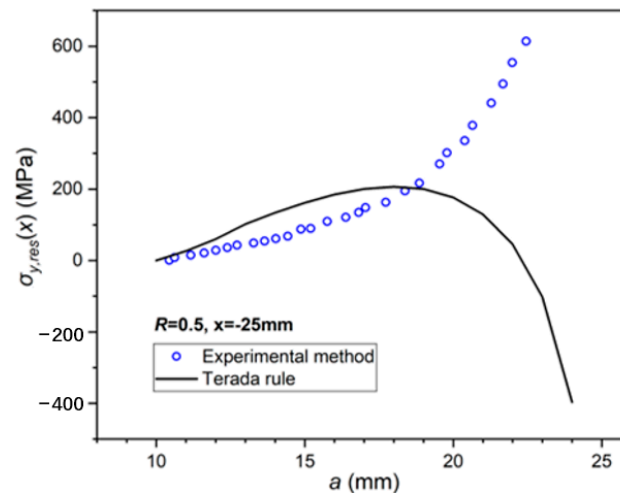


Figure 7. Experimental and theoretical results of residual stress.

2.3.3. Impact of Cyclic Loading on Residual Stress Distribution

To analyze the impact of cyclic loading on longitudinal residual stresses, The WRS variation without pre-cracked butt joint specimens under cyclic loading was measured, as shown in Figure 8, where the vertical axis represents the change value of longitudinal welding residual stress re-distribution. From Figures 7 and 8, throughout the cyclic loading process, the change in WRS in the butt specimen without pre-cracks is much smaller than that in the butt specimen with pre-cracks. The reason for this is that there are significant changes in residual stress when the sum of the applied stresses and the residual stresses locally exceeds the material's yield strength before the cracks appear. In this study, the sum of the applied and residual stresses is less than the material yield strength. Therefore, the cyclic loadings have little influence on the WRS distribution.

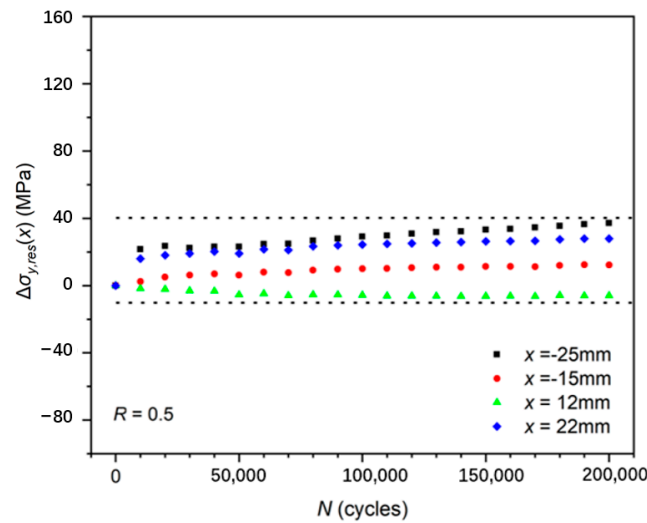


Figure 8. Variation in longitudinal residual stress of the MT specimens without pre-cracks with the number of cyclic loadings.

3. Finite Element Analysis

3.1. Import of Initial Welding Residual Stress

The initial longitudinal WRS measured via X-ray was imported into the FE model, as shown in Figure 9. It is assumed that the material’s properties of the base and welding material are the same to simplify the calculation [17]. The import processes of initial WRS are as follows: (1) meshing the model and dividing several sets of elements by identical abscissa x ; (2) compiling keyword instructions to assign longitudinal initial WRS to the element’s sets; (3) setting boundary conditions and performing self-balance calculation. The initial WRS distribution, as shown in Figure 10, represents the residual stress distribution of the model after self-balance.

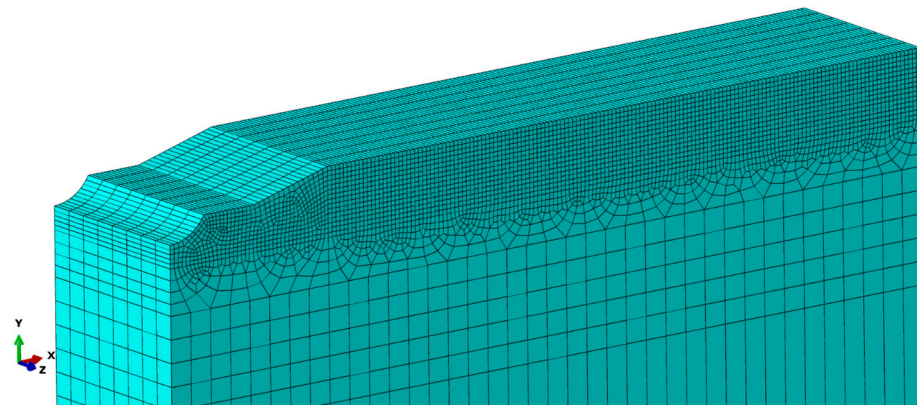


Figure 9. Meshing scheme of MT specimen (1/4 model).

To verify whether the initial WRS distribution on the FE model was acceptable, the average of initial WRS data of the butt specimen measured via X-ray with pre-cracks was compared with the FE model’s results after self-balance, as is shown in Figure 11, where the shaded areas indicate the standard error bars of the test measurements. According to Figure 11, the stress distribution after self-balance is close to the actual measured results in terms of magnitude and characteristics, as a result of which the initial WRS field obtained from the simulation is considered to be accurate and can be used as the initial state for the subsequent re-distribution behavior and crack propagation simulation study.

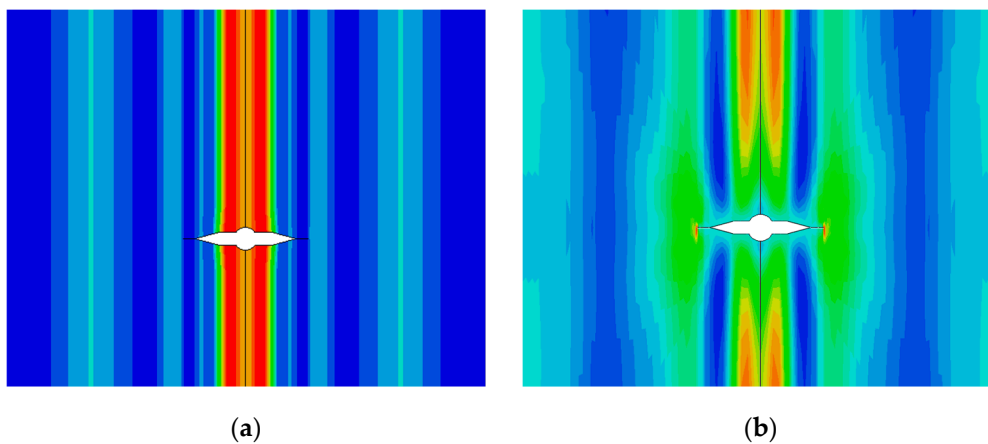


Figure 10. Initial WRS distribution in FE model: (a) before self-balance; (b) after self-balance.

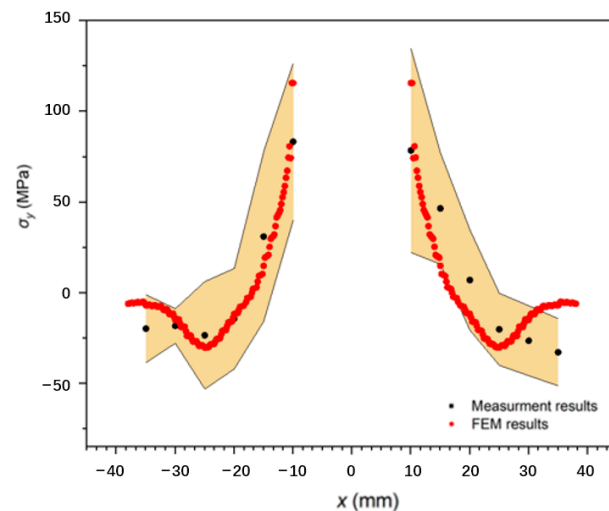


Figure 11. Measurement and simulation results of the initial longitudinal WRS.

3.2. Residual Stress Intensity Factor K_{res} by XFEM

According to the empirical formula of SIF in fracture mechanics [18], when the crack increment is small, the value of SIF changes little and can be assumed to be a constant. This study assumes that SIF in the crack tip is constant during each crack increment. The elastic–plastic simulation method of continuous crack propagation considering WRS redistribution is based on the extended finite element method (XFEM). The procedures of the simulation are shown in Figure 12.

The procedures of this simulation method are as follows:

- Import the initial stress distribution into the FE model (in Section 3.1).
- Calculate the stress–strain value for the first crack increment step under cyclic loadings, although all elements' numbers will be kept the same following the initial increment step.
- Update the crack length according to the experimental data.
- Read the stress–strain state of each element under the previous crack length and assign it to the current model.
- Extract the K_{res} at the crack tip of each increment using J-integral.

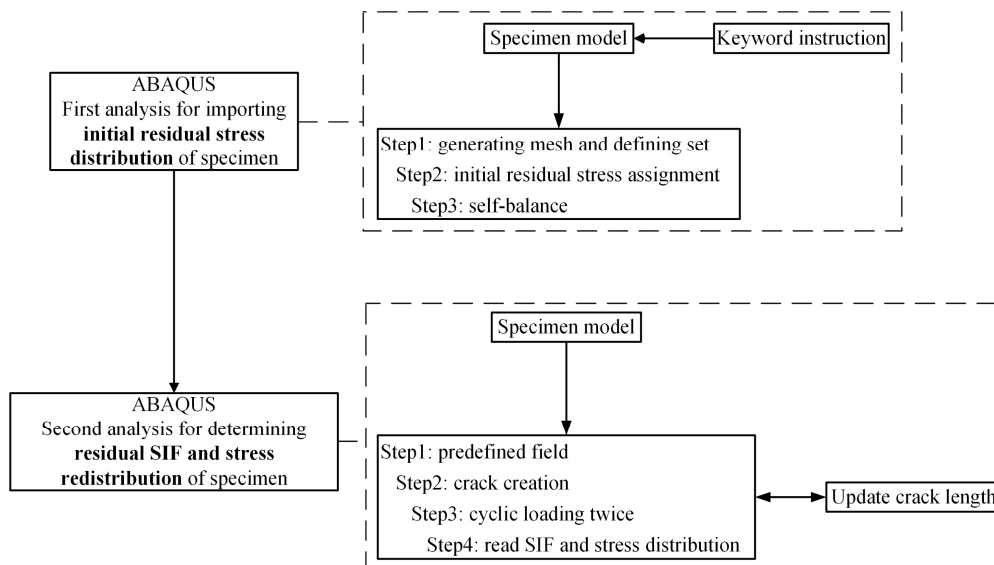


Figure 12. Steps of elastic–plastic finite element simulations.

All convergent contour results average the final calculation result. It should be noted that when reading the K_{res} , the external load has been unloaded to 0.

3.3. Effect of Cyclic Loadings on the Simulation Results

As shown in Figure 13, longitudinal WRS distribution near the crack tip changes significantly after the first cycle of loading ($N = 0$ vs. $N = 1$), and the peak residual stresses are biased away from the crack tip. However, the distribution hardly varies further when the number of cycles increases ($N = 2$ to $N = 10$). This phenomenon indicates that the re-distribution behavior of residual stresses in loading cycles occurs in the first cycle. This phenomenon occurs because the significant changes in the longitudinal WRS distribution during the first cycle are associated with the quasi-static relaxation effects caused by the applied load in the same direction as the residual stress. Therefore, in the elastic–plastic simulation of fatigue crack propagation, it is necessary to make the finite element model undergo at least one complete cyclic loading before obtaining the residual stress distribution and K_{res} .

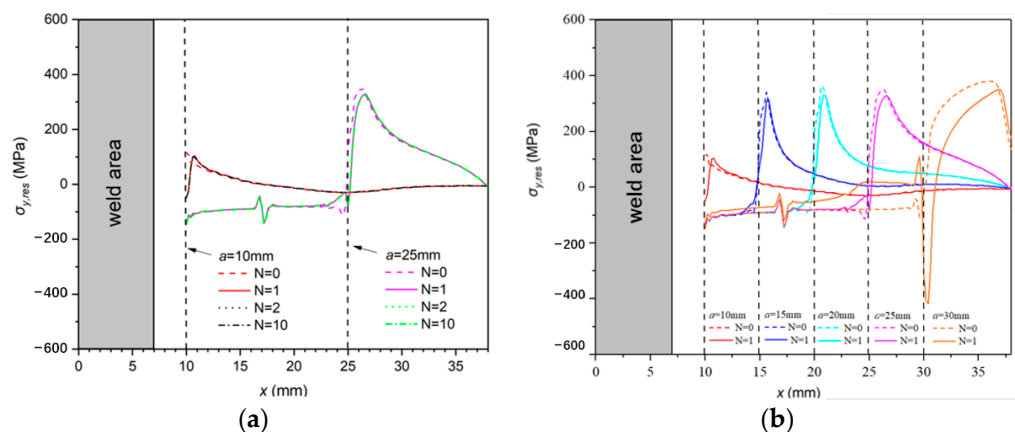


Figure 13. Influence of fatigue load cycles on residual stress: (a) different numbers of cycles; (b) different crack lengths.

3.4. Simulation Results and Comparison

The traditional static import simulation method and the continuous dynamic one established in this study are used to calculate the longitudinal WRS re-distribution on

the crack extension line with different crack lengths at $R = 0.1$, which are compared with the experimental results at $x = -25$ mm, as shown in Figure 14. The dynamic simulation method means that the crack length and stress field are constantly updated according to Figure 12 to obtain the dynamic variation in residual stress with cyclic loading. On the other hand, the static simulation method refers to a static method that does not consider WRS re-distribution during the loading process, given an initial predefined field and a certain defined crack length.

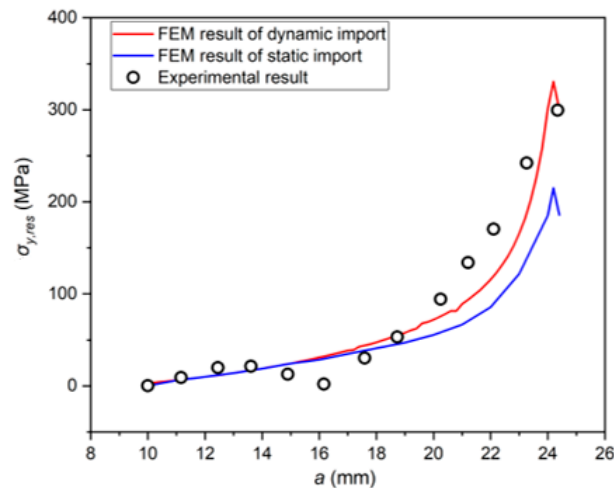


Figure 14. Experimental and simulation results of longitudinal WRS ($R = 0.1$).

It can be seen from Figure 14 that the calculation results of two finite element methods are close to each other in the front and middle sections of the curve. The static method’s results are significantly smaller in the curve’s rear section than the dynamic and experimental data. The main reason for this phenomenon is that the static method does not consider plastic re-distribution behavior during crack propagation. When the crack length is short, crack tip plasticity does not affect the measuring point. Therefore, the elastic component of re-distribution is dominant, and the three methods have few differences. However, the plastic component increases simultaneously when the plastic zone is gradually close to the measuring point.

Considering the plasticity, the elastic–plastic continuous dynamic simulation method is closer to the experimental results. This phenomenon indicates that the method established in this study can obtain a more accurate residual stress field re-distribution behavior.

4. Residual Stress Intensity Factor K_{res}

4.1. Comparison between WFM and FEM

The weight function method (WFM) based on [19,20] is commonly used to quantify the effect of residual stress distribution and estimate residual stress SIF K_{res} . The K_{res} calculation equation for WFM is as follows,

$$K_{res,+a} = \int_0^a \sigma_y(x)h(a,x)dx \tag{8}$$

where $h(a,x)$ is a weight function that depends on the crack length a and the abscissa x .

This study uses three kinds of $\sigma_y(x)$ distribution function. They are the Terada distribution function, the Tada and Paris distribution function, as shown in the previous

Section 2.3.1, and a segmented approximation function (SAF) distribution based on measured data, which can be expressed as

$$\sigma_y(x) = \begin{cases} 19.21x + 83.18 & 0 \leq x \leq 2.5 \\ -38.91x + 228.48 & 2.5 \leq x \leq 6.5 \\ 10.12x - 90.19 & 6.5 \leq x \leq 11.5 \\ -4.43x + 77.09 & 11.5 \leq x \leq 24.5 \\ 2.37x - 89.51 & 24.5 \leq x < 38 \end{cases} \quad (9)$$

Meanwhile, the $K_{res}-2a/W$ curve is calculated and summarized based on the elastic-plastic FE simulation in Section 3.2, which is compared with the calculation results of WFM above, as shown in Figure 15.

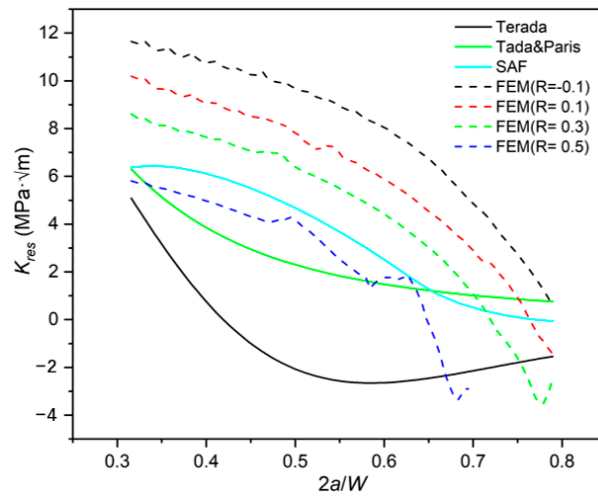


Figure 15. Comparison of calculation results between WFM and simulation method.

According to Figure 15:

- The magnitudes of K_{res} predicted using WFM and the FE method are similar, all in the range of $-4 \sim 12 \text{ MPa} \cdot \text{m}^{1/2}$. At the same time, WFM neglects the effect of plastic deformation on residual stress near the crack tip, resulting in a different trend.
- With the crack length increase, K_{res} calculated using all methods shows a decreasing trend, except for that using the Terada distribution. Combined with the initial WRS distribution in Figure 5, it is speculated that the increase in K_{res} may be related to the overestimation of peak compressive stress when using the Terada distribution. The K_{res} curve predicted using Terada distribution increased near $2a/W = 0.55$, where the initial residual stress is precisely located near the right side of the compressive stress peak, raising K_{res} corresponding to the release of compressive stress during crack propagation.
- The calculation results of WFM depend on the choice of the initial distribution function. Weight function adopting initial distribution SAF, like that in the FE model, obtains the closest results to the simulation method. At the same time, there is a significant difference between the results of the Terada and Tada and Paris functions. This phenomenon indicates that when predicting K_{res} , the accuracy significantly depends on the initial distribution.
- With the increase in $2a/W$, there is a significant difference between WFM and simulation results. It can be seen from Figure 15 that the trend of the $K_{res}-2a/W$ curves of the WFM tends to be stable no matter what initial distribution is used. The influence of the elastic-plastic behavior of the material causes this phenomenon. When the local stress is close to the fracture limit, a significant yield area occurs on the specimen, resulting in its re-distribution behavior being entirely dominated by plasticity. Crack

tips and surfaces are subjected to the compression of the plastic zone after unloading, and the K value extracted by the J-integral gradually decreases. However, WFM is based on linear elasticity assumption, considering that the residual ligament of the specimen is too short to lead to the general release of residual stress. In addition, the influence of plastic re-distribution of residual stress on crack tip is not considered in WFM. Therefore, WFM cannot predict the rapid decrease in K_{res} when the specimen approaches the fracture toughness.

- The $K_{res}-2a/W$ curves calculated using the simulation considering the elastic–plastic response of materials show a significant stress ratio effect, which WFM cannot predict.

4.2. The Stress Ratio Effect of K_{res}

As seen from Figure 16, with the increase in stress ratio R , the $K_{res}-2a/W$ curve calculated using the simulation method shifts downward, while the variation trend of the $K_{res}-2a/W$ curve at different stress ratios is the same. Therefore, it can be considered that the intercept of the $K_{res}-2a/W$ curve is related to the stress ratio R .

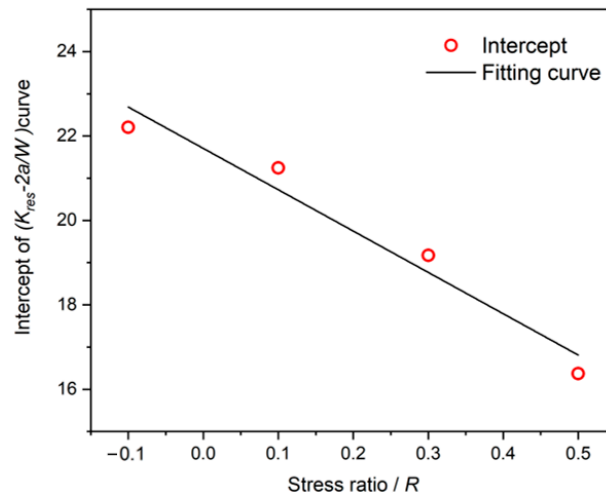


Figure 16. Intercept of $K_{res}-2a/W$ curve VS stress ratio R .

As shown in Figure 16, the intercept of the $K_{res}-2a/W$ curve shows a strong linear relationship with stress ratio R . Therefore, it is assumed that the $K_{res}-2a/W$ curve is linear with the decreasing offset degree of stress ratio R in this study. The $K_{res}-2a/W$ curve is fitted using a cubic polynomial based on the calculation results of the FEM. The fitting model is expressed as follows:

$$K_{res} = 23.821 - 9.791R - 80.795\left(\frac{2a}{W}\right) + 168.268\left(\frac{2a}{W}\right)^2 - 133.694\left(\frac{2a}{W}\right)^3 \quad (10)$$

As shown in Figure 17, the predicted results of the fitted model at different stress ratios are in general agreement with FEM results, with slight errors only when $2a/W$ is large (corresponding to the late stage of crack propagation). The main reason for this phenomenon is that when the crack length approaches the maximum stable growth length of the specimen, the specimen will undergo an extensive range of plastic yield. At this time, the crack surface is subjected to compressive stresses from the plastic zone at the crack tip, resulting in a low negative value of K_{res} calculated by FEM. In general, the prediction deviation of the fitted model is acceptable due to the small magnitude of K_{res} . Therefore, for the MT specimens in this study, it is proven that the fitted model predicts K_{res} well.

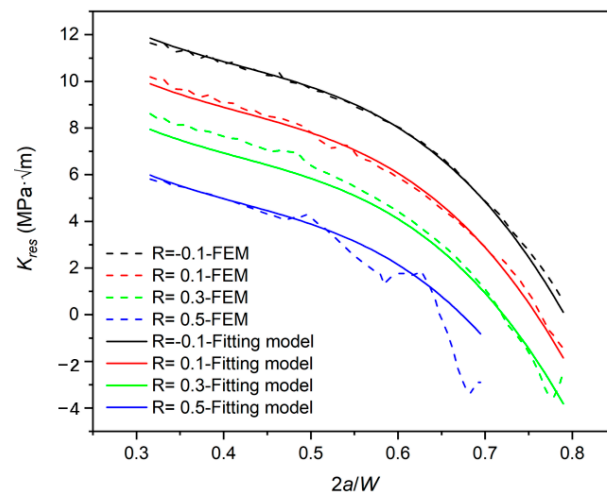


Figure 17. Comparison between the results of fitting model and FEM.

5. Conclusions

This study uses theoretical, experimental, and finite element methods to study the re-distribution behavior of welding residual stress in Ni-Cr-Mo-V steel butt-welded specimens during crack propagation. For MT butt-welded specimens, the initial residual stress was measured, and a series of crack propagation experiments were conducted. The specimen's residual stress intensity factor, K_{res} , was calculated using the weight function method and elastic-plastic continuous crack propagation simulation procedure established in this study. According to the results of theoretical, experimental, and finite element methods, the following conclusions can be drawn:

1. The accuracy of the weight function method depends on the selection of the initial distribution function. Meanwhile, the stress ratio effect of K_{res} cannot be predicted using the weight function method.
2. Terada's re-distribution rule overestimates the increment of longitudinal residual stresses, and it is not suitable for predicting the re-distribution of residual stresses in marine high-tensile steel.
3. Compared with the Terada re-distribution rule and static simulation method with initial distribution, the elastic-plastic continuous simulation method considering load timing is more consistent with the experimental measurements, which indicates that the plastic re-distribution behavior should be considered in the simulation of fatigue crack propagation.
4. The K_{res} values calculated using elastic-plastic continuous simulation procedure indicate that K_{res} is affected by the crack size a/W , and exhibits a noticeable stress ratio effect when the applied stress amplitude is kept constant, which is not reflected by WFM.
5. The K_{res} fitting model related to a/W considering the stress ratio effect is established, and the results are in good agreement with the finite element calculation results, which can better reflect the WRS plastic re-distribution behavior.

Author Contributions: Writing—original draft preparation, Y.X., J.L. and K.Y.; writing—review and editing, J.Y. and Y.G. All authors have read and agreed to the published version of the manuscript.

Funding: The National Natural Science Foundation of China funded this research (No. 52171320).

Informed Consent Statement: Informed consent was obtained from all subjects involved in the study.

Data Availability Statement: The data presented in this study are available on request from the corresponding author. No new data were created or analyzed in this study. Data sharing is not applicable to this article.

Conflicts of Interest: The authors declare no conflict of interest.

Nomenclature

a	current crack length
a_0	initial crack length
E	Young's modulus
h	specimen length
R	loading/stress ratio
W	specimen width
ν	Poisson's ratio
CT	compact tension (specimen)
FE(M)	finite element (method)
LEFM	linear elastic fracture mechanics
MT	middle tension (specimen)
SIF	stress intensity factor
WFM	weight function method
WRS	welding residual stress
XFEM	extended finite element method
$C_1, C_2, \gamma_1, \gamma_2$	the Chaboche combined hardening model constants
K_{res}	residual stress intensity factor
ΔK_{eff}	effective stress intensity factor range
σ_0	initial yield strength
$\Delta\sigma_{nominal}$	nominal stress range
σ_y	initial longitudinal welding residual stress
$\sigma_{y,0}$	the maximum welding residual stress at the center line of the welding
$\sigma_{y,res}$	longitudinal welding residual stress
$\Delta\sigma_{y,res}$	change in longitudinal residual stress
σ_{ys}	yield strength
σ_u	ultimate tension strength
$h(a,x)$	weight function

References

- Adiban, S.; Ramu, M. Study on the effect of weld defects on fatigue life of structures. *Mater. Today Proc.* **2018**, *5*, 17114–17124. [[CrossRef](#)]
- Edwards, L. Influence of residual stress re-distribution on fatigue crack growth and damage tolerant design. *Mater. Sci. Forum.* **2008**, *524–525*, 363–372.
- Servetti, G.; Zhang, X. Predicting fatigue crack growth rate in a welded butt joint: The role of effective R ratio in accounting for residual stress effect. *Eng. Fract. Mech.* **2009**, *76*, 1589–1602. [[CrossRef](#)]
- Barsoum, Z.; Barsoum, I. Residual stress effects on fatigue life of welded structures using LEFM. *Eng. Fail. Anal.* **2009**, *16*, 449–467. [[CrossRef](#)]
- Lee, C.S.; Kim, M.H.; Lee, J.M.; Mahendran, M. Computational study on the fatigue behaviour of welded structures. *Int. J. Plast.* **2011**, *20*, 423–463.
- Terada, H. *Stress Intensity Factor Analysis and Fatigue Behaviour of a Crack in the Residual Stress Field of Welding*; ASTM International: West Conshohocken, PA, USA, 2007.
- Xu, X. *Effects of Residual Stress on Surface Crack Growth at Welded Joints*; Dalian University of Technology: Dalian, China, 2013. (In Chinese)
- Liljedahl, C.; Zanellato, O.; Fitzpatrick, M.; Lin, J.; Edwards, L. The effect of weld residual stresses and their re-distribution with crack growth during fatigue under constant amplitude loading. *Int. J. Fatigue* **2010**, *32*, 735–743. [[CrossRef](#)]
- Liljedahl, C.; Brouard, J.; Zanellato, O.; Lin, J.; Tan, M.; Ganguly, S.; Irving, P.E.; Fitzpatrick, M.; Zhang, X.; Edwards, L. Weld residual stress effects on fatigue crack growth behaviour of aluminium alloy 2024-T351. *Int. J. Fatigue* **2009**, *31*, 1081–1088. [[CrossRef](#)]
- Liljedahl, C.; Tan, M.; Zanellato, O.; Ganguly, S.; Fitzpatrick, M.; Edwards, L. Evolution of residual stresses with fatigue loading and subsequent crack growth in a welded aluminium alloy middle tension specimen. *Eng. Fract. Mech.* **2008**, *75*, 3881–3894. [[CrossRef](#)]
- Wang, L.; Qian, X. Welding residual stresses and their relaxation under cyclic loading in welded S550 steel plates. *Int. J. Fatigue* **2002**, *162*, 106992. [[CrossRef](#)]
- Moshtaghi, H.; Safyari, M. Effect of Work-Hardening Mechanisms in Asymmetrically Cyclic-Loaded Austenitic Stainless Steels on Low-Cycle and High-Cycle Fatigue Behavior. *Steel Res. Int.* **2021**, *92*, 2000242. [[CrossRef](#)]

13. Moshtaghi, M.; Loder, B.; Safyari, M.; Willidal, M.; Hojo, T.; Mori, G. Hydrogen trapping and desorption affected by ferrite grain boundary types in shielded metal and flux-cored arc weldments with Ni addition. *Int. J. Hydrogen Energy* **2022**, *47*, 20676–20683. [[CrossRef](#)]
14. *E 647-08*; ASTM Standard Test Method for Measurement of Fatigue Crack Growth Rates. ASTM International: West Conshohocken, PA, USA, 2015.
15. Terada, H. An analysis of the stress intensity factor of a crack perpendicular to the welding bead. *Eng. Fract. Mech.* **1976**, *8*, 441–444. [[CrossRef](#)]
16. Tada, H.; Paris, P.C. The stress intensity factor for a crack perpendicular to the welding bead. *Int. J. Fract.* **1983**, *21*, 279–284. [[CrossRef](#)]
17. Qiang, B.; Li, Y.; Yao, C.; Wang, X. Through-thickness welding residual stress and its effect on stress intensity factors for semi-elliptical surface cracks in a butt-welded steel plate. *Eng. Fract. Mech.* **2018**, *193*, 17–31. [[CrossRef](#)]
18. Perez, N. Fatigue Crack Growth. In *Fracture Mechanics*; Springer International Publishing: Cham, Switzerland, 2017; pp. 327–372.
19. Rice, J.R. Some remarks on elastic crack-tip stress fields. *Int. J. Solids Struct.* **1972**, *8*, 751–758. [[CrossRef](#)]
20. Bueckner, H. Novel principle for the computation of stress intensity factors. *Z. Angew. Math. Phys.* **1970**, *50*, 529–546.

Disclaimer/Publisher’s Note: The statements, opinions and data contained in all publications are solely those of the individual author(s) and contributor(s) and not of MDPI and/or the editor(s). MDPI and/or the editor(s) disclaim responsibility for any injury to people or property resulting from any ideas, methods, instructions or products referred to in the content.